







Single crystal growth of superconducting UTe_2 by molten salt flux method

H. Sakai ^{*}, P. Opletal , Y. Tokiwa , E. Yamamoto, Y. Tokunaga , S. Kambe, and Y. Haga [†]
Advanced Science Research Center, Japan Atomic Energy Agency, Tokai, Ibaraki 319-1195, Japan

 (Received 4 April 2022; accepted 5 July 2022; published 29 July 2022)

The molten salt flux method is applied as a synthetic route for the single crystals of the spin-triplet superconductor UTe_2 . The single crystals under an optimized growth condition with excess uranium exhibit a superconducting transition at $T_c = 2.1$ K, which is the highest T_c reported for this compound. The obtained crystals show a remarkably large residual resistivity ratio with respect to the room temperature value and a small residual electronic contribution in specific heat well below T_c . These results indicate that the increase of T_c in UTe_2 can be achieved by reducing the disorder associated with uranium vacancies. The excess uranium in the molten salt acts as a reducing agent, preventing tetravalent uranium from becoming pentavalent and suppressing creation of uranium vacancies. At the same time, the relatively low growth temperature can suppress Te volatilization.

DOI: [10.1103/PhysRevMaterials.6.073401](https://doi.org/10.1103/PhysRevMaterials.6.073401)

I. INTRODUCTION

Uranium ditelluride (UTe_2) has attracted considerable attention since the compound exhibits a number of novel superconducting (SC) features. Ran *et al.* [1] first reported that UTe_2 exhibits an unconventional superconductivity below $T_c = 1.6$ K, and extremely large upper critical field H_{c2} exceeding the Pauli-limiting field. A short time later, by applying the strong magnetic field (H) over ~ 40 T reentrant SC phase was found [2,3]. The magnetic susceptibility of UTe_2 above T_c is quite anisotropic with the easy axis along the a axis, and no magnetic order is seen [4]. By applying hydrostatic pressure, however, multiple SC and magnetic ordered phases were observed [5–8], indicating that the system is located on the verge of quantum criticality. Furthermore, the formation of spin-triplet SC pairing has been experimentally suggested from considerably small decrease in the nuclear magnetic resonance (NMR) shift below $T_c(H)$ under ambient pressure [9–11].

To grow single crystals of UTe_2 , the chemical vapor transport (CVT) or tellurium flux (Te-flux) method is usually used [12–14]. The highest T_c of 2 K was observed in the single crystals grown by the CVT method [15]. For the CVT method, however, the T_c value occasionally varies from piece to piece within a batch; in some cases, the T_c value is even spatially distributed within a single piece [16]. At the earlier stage, a large residual electronic contribution $\gamma_0 = C_e/T$ ($T \rightarrow 0$) in specific heat well below T_c was reported for a CVT-grown SC sample with $T_c = 1.6$ K to be approximately half of the normal state value γ_n [1]. This large γ_0 value was initially suggested to be an intrinsic feature of UTe_2 with a large fraction of ungapped electronic states. However, the improvement of sample quality led to an increase of the T_c value accompanied by a decrease of residual γ_0 [17,18]. The γ_0 value was reduced

to $\sim 20\%$ of γ_n for the crystals with $T_c = 2$ K grown by the CVT method [15]. For UTe_2 , it is theoretically proposed that a finite amount of γ_0 would remain even assuming extremely low impurity scattering, but the residual density of states well below T_c becomes smaller for samples with higher T_c [19].

Another measure of the quality of metallic samples is the residual resistivity ratio (RRR). Although it often reaches 100 or more for single crystals of various uranium-based intermetallic compounds, it is yet less than 100 at most even for the CVT-grown crystals of UTe_2 with high $T_c = 2$ K [15]. This suggested that there would be still room to increase T_c if we could prepare higher quality single crystals with a larger RRR value.

In general, to further improve sample quality, some defects or deficiencies remaining in crystals must be reduced. For UTe_2 , Te deficiency was initially considered to be a key source to induce superconductivity [17]. However, we recently found that the U stoichiometry is more important for obtaining SC crystals [4,20]; a few percent vacancies on the U sites completely suppress the superconductivity in UTe_2 . In this paper, we report the molten salt flux (MSF) method as a route to grow high-quality single crystals of UTe_2 with minimal U vacancies. Such stoichiometric UTe_2 crystals grown by the MSF method exhibit the highest T_c of 2.1 K with a remarkably large RRR ~ 1000 .

II. EXPERIMENTAL METHODS

In the MSF method, an equimolar mixture of sodium chloride and potassium chloride ($\text{NaCl} + \text{KCl}$) was chosen, which has a eutectic melting point of about 650°C [21]. Prior to use, pieces of natural U metal (purity $>99.99\%$) [22] were cleaned in nitric acid to remove surface oxides. The weight of each piece ranged from 0.2 to 0.5 g. In each growth procedure, a piece of lightly etched U metal and granule of Te metal (purity 99.9999%, Rare Metallic Co. Ltd., Tokyo, Japan) were weighed to adjust the target molar ratio of Te/U. Then, the metals were placed together in the bottom of a carbon

^{*}sakai.hironori@jaea.go.jp

[†]haga.yoshinori@jaea.go.jp

crucible with an inner and outer diameter of 13 and 15 mm, respectively, and a length of 70 mm, which was made by machining from a carbon rod. The equimolar mixture of NaCl (purity 99.995%, Kanto Chemical Co. Inc., Tokyo, Japan) and KCl (purity 99.999%, Merck Co. Inc., Kenilworth, NJ, USA) was weighed, then well ground, and mixed using a mortar and pestle. The salt mixture was then added into the carbon crucible and packed with quartz wool to prevent spillage.

The carbon crucible filled with the metals and salt mixture was placed in a quartz tube with an inner and outer diameter of 15 and 18 mm, respectively. It was heated at 200 °C for several hours under dynamic vacuum to dehydrate the contents. Then, the carbon crucible was vacuum-sealed into the quartz tube. The sealed quartz tube was inserted into a home-built vertical electric tube furnace. First, it was preheated at 450 °C for 24 h, then raised to 950 °C over 24 h, and kept for 24 h to produce a uniform melt. Then, the temperature was slowly lowered to a final-step temperature (T_f) with a ramp rate of 0.02–0.03 °C per min. The temperature was maintained at T_f for 24 h for annealing. After cooling down, the molten salts were easily dissolved in water, and the millimeter-sized crystals were picked up, washed with ethanol, and immediately dried in a vacuum atmosphere. The salt solution remaining after the crystals were removed contained a number of microcrystals; thus it was filtered through a filter paper.

The crystallographic structures of the samples were determined at room temperature by single crystal x-ray diffraction (XRD) with a graphite monochromated Mo K_α radiation. The scattered x-ray beam was recorded on an imaging plate detector (R-AXIS RAPID, Rigaku Corp., Tokyo, Japan). Absorption correction with the empirical method was applied prior to the structural solution. Structural solution and crystallographic parameters fitting were performed using the SHELX program [23]. Electron-probe microanalysis (EPMA) was performed using wavelength-dispersive spectrometers installed in a scanning electron microscope (SEM) (JXA-8900, JEOL Ltd., Tokyo, Japan).

Electrical resistivity was measured using the ac four-probe method with a current of 1–10 mA at a frequency of 90–190 Hz in a closed-cycle refrigerator (SHI-950T, Janis Research Co., Wilmington, MA, USA), which can reach a temperature of as low as 1.2 K. The electrical contacts were made by 25- μ m-diameter gold wires spot-welded on a flat facet of the crystal. Magnetization (M) was measured using a commercial superconducting quantum interference device magnetometer (MPMS XL7, Quantum Design, Inc., San Diego, CA, USA) in the temperature range of 2–300 K with the application of a magnetic field of 10 kOe. Specific heat was measured using the heat relaxation method with a home-built calorimeter installed in a ^3He cryostat (HelioxVT, Oxford Instruments, Abingdon, UK), or in a ^3He - ^4He dilution fridge (TS-3H100-STD, Taiyo Nippon Sanso Corporation, Tokyo, Japan).

III. RESULTS AND DISCUSSIONS

A. CVT method

For comparison, single crystals were prepared by the CVT method using iodine as the transport agent [20]. The growth

TABLE I. Summary of the CVT-grown UTe_2 single crystals [20]. The first column is the sample batch name. Te/U is the starting molar ratio. The applied temperature gradient is indicated by T_L and T_H . T_c^{onset} is defined as the onset of resistivity drop. RRR refers to the residual resistivity ratio of $\rho(300\text{ K})/\rho(0)$ with regard to $\rho(0)$ which is estimated by fitting to $\rho(T) = AT^2 + \rho(0)$ in the range of $T_c \leq T \leq 4\text{ K}$. The values of T_c^{onset} and RRR are presented as representative values measured on several crystals from the same batch.

Sample	Te/U	T_L (°C)	T_H (°C)	T_c^{onset} (K)	RRR
NS	2	850	950	<0.45	2
SC1	1.8	1000	1050	1.52–1.63	15–30
SC2	1.8	850	950	1.75–1.90	20–30

method was described in the Appendix. Let us briefly summarize the single crystal growth of UTe_2 by the CVT method. The experimental conditions for the CVT growth in this work are listed in Table I. The values of T_c and RRR for each representative sample are given.

When the starting Te/U ratio was adjusted to the stoichiometric value of 2, as denoted in Sec. I, the obtained sample (labeled as NS) did not show superconductivity at a temperature of as low as 0.45 K. Generally, in the case of CVT growth for SC single crystals of UTe_2 , an excess amount of uranium must be added into the quartz ampule, i.e., the prepared Te/U ratio should be 1.5–1.8 in the U-rich (conversely, Te-poor) condition with respect to the stoichiometric ratio of 2. The lower temperature gradient by higher temperature T_H and lower T_L in the furnace yields UTe_2 crystals with higher T_c . The threshold of T_L appears to be about 700 °C, as the further lowering of T_L could not yield any SC crystals [15]. As reported by Haga *et al.* [20], the NS crystal is most likely uranium-deficient $\text{U}_{0.96}\text{Te}_2$, whereas the SC samples of SC1 and SC2 are close to the stoichiometric composition with an accuracy of $\sim 1\%$.

The CVT and Te-flux methods tend to yield U-deficient $\text{U}_{1-\delta}\text{Te}_2$. In the CVT growth, not only temperature gradient, but also chemical pressure gradient of each chemical species needs to be optimized, which makes it difficult to control nonstoichiometry in the nonequilibrium process. Similarly, in the case of the Te-flux method, the crystals show no superconductivity or superconductivity with lower T_c [12–14]. It is expected for uranium to be deficient in the Te-flux method because the prepared Te/U ratio must be considerably larger than 2, and the Te-rich molten phase [24] requires a high temperature of more than 950 °C to obtain the UTe_2 phase.

Figure 1 shows the temperature dependence of normalized resistivity $\rho(T)/\rho(300\text{ K})$ along the a axis for the representative single crystals of NS, SC1, and SC2. The RRR value was estimated using the $\rho(0)$ obtained by fitting to $\rho(T) = AT^2 + \rho(0)$ in the range of $T_c \leq T \leq 4\text{ K}$, assuming a Fermi-liquid state just above T_c . The $\rho_a(0)$ of the NS crystal in Fig. 1 was 2.2 m Ω cm, whereas that of the SC2 was 34 $\mu\Omega$ cm. The considerably higher residual resistivity of the NS crystal indicates higher density of its scattering centers.

$\text{U}_{1-\delta}\text{Te}_2$ may be described as $\text{U}_{1-5\delta}^{4+}[\text{V}_U]_\delta\text{U}_{4\delta}^{5+}\text{Te}_2^{2-}$, where $[\text{V}_U]$ means the vacancies of U sites. A $[\text{V}_U]$ of $\sim 4\%$ in the NS crystal significantly changes the $5f$ electron count because of

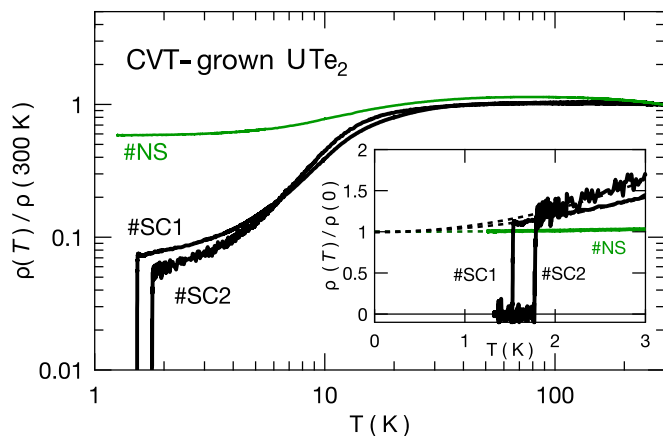


FIG. 1. Temperature dependence of normalized resistivity, $\rho(T)/\rho(300 \text{ K})$, for the CVT-grown single crystals of UTe_2 . The resistivity is measured along the a axis. The inset shows the enlarged plot of $\rho(T)/\rho(0)$ with regard to $\rho(0)$ in the low-temperature part. The value of $\rho(0)$ was estimated by fitting to $\rho(T) = AT^2 + \rho(0)$ in the range of $T_c \leq T \leq 4 \text{ K}$.

the simultaneous generation of U^{5+} and U vacancies which cause strong scattering of conduction electrons. Therefore, even if the uranium deficiency of the SC crystals is less than 1%, extra electron scattering may occur, and/or the corresponding residual density of states may exist in the SC state.

B. MSF method

The MSF method is extensively used for the synthesis of lanthanide oxides, borides, and chalcogenides. In particular, the equimolar $\text{NaCl}+\text{KCl}$ flux is known to dissolve uranium well and has been proposed as a solvent for the electrochemical recovery of uranium metal from spent nuclear fuel [25–27]. Since the U(IV) chloride is easily reduced to U(III) with excess uranium metal in the salt [25], the MSF

method with a surplus of uranium would be suitable to prevent U(IV) in UTe_2 from being partially oxidized to U(V) . Another advantage of the MSF method is that crystals can be obtained at relatively low temperatures to avoid volatilization of the constituent chalcogens.

We attempted to start the MSF growth from the same Te/U ratio of 1.8 as used in the CVT method. It is labeled as M6 in Table II. The molar ratio of salt for M6 was 21 with regard to the U amount. To increase the homogeneity of the sample, the product was annealed for 24 h at $T_f = 650 \text{ }^\circ\text{C}$ in the vacuum quartz tube. After dissolving the salt in water, many needlelike crystals with a length of 2–10 mm and a thickness of about 0.5–1 mm were obtained. They were, however, not UTe_2 crystals but hexagonal U_7Te_{12} , which was reported as a ferromagnet by magnetization measurement using a polycrystalline sample [28]. Because U_7Te_{12} can be formally regarded as the mixed valence compound $\text{U(III)}_4\text{U(IV)}_3\text{Te}_{12}$, we can say that the MSF method actually yielded a type of reduced U(III) species in the system. Note that $\text{Te/U} = 1.714 \dots$ of U_7Te_{12} was close to the starting composition of $\text{Te/U} = 1.8$ for M6.

The semimetallic resistivity in the milliohm-centimeter range for the crystal of U_7Te_{12} is confirmed, and a kink in resistivity is observed at $T_{\text{Curie}} = 47 \text{ K}$ (not shown). We could obtain the U_7Te_{12} crystals prepared from $\text{Te/U} = 1.71$, which is labeled as M7. The ferromagnetism at T_{Curie} is confirmed by the magnetization measurement. The detailed physical properties for U_7Te_{12} using the single crystals will be separately reported.

To obtain the UTe_2 phase, the Te/U ratios were from 2.0 down to 1.9, as listed in Table II (M1, M2, M3, M4, and M5). We attempted the batches of H1, H2, L1, and L2 to investigate the set of several final steps and annealing temperatures T_f . The amount of salt was varied in some cases. Several crystals in each batch were investigated by electrical resistance measurement to evaluate the T_c value and quality of samples.

TABLE II. Summary of the MSF-grown UTe_2 single crystals in this work. The first column is the sample batch name. The columns of Te/U and Salt/U mean starting and salt molar ratios, respectively. Major and minor products (if included) are indicated. When the resistivity measurements using crystals of UTe_2 were performed, the values of T_c^{onset} defined as the onset of resistivity drop and the RRR, $\rho(300 \text{ K})/\rho(0)$ are displayed with regard to $\rho(0)$, which is estimated by fitting to $\rho(T) = AT^2 + \rho(0)$ in the range of $T_c \leq T \leq 4 \text{ K}$. The values of T_c^{onset} and RRR are presented as representative values measured on several crystals from the same batch. Short annotations are added to the last column when necessary.

Sample	Te/U	Salt/U	T_f ($^\circ\text{C}$)	Major	Minor	T_c^{onset} (K)	RRR	Note
M1	2.0	29	650	UTe_2	–	1.7–1.8	40–60	
M2	1.93	37	650	UTe_2	–	1.9–2.0	60–80	
M3	1.92	36	650	UTe_2	–	1.95–2.1	30–40	
M4	1.90	40	650	UTe_2	–	1.8–1.95	50–60	
M5	1.90	67	650	UTe_2	–	1.9–2.05	50–60	
M6	1.8	21	650	U_7Te_{12}	–	–	–	
M6a	1.8	40	650	U_7Te_{12}	UTe_2^a	2.0–2.1 ^a	80–130 ^a	^a Small isolated crystals
M7	1.71	60	650	U_7Te_{12}	UTe_2^b	2.1 ^b	170–1000 ^b	^b Small isolated crystals
H1	2.0	48	700	UTe_2	–	1.6	11–12	Centrifuged
H2	1.95	42	700	UTe_2	–	1.75–1.9	35–60	
L1	1.95	38	600	UTe_2	–	1.6–1.8	20–30	
L2	1.90	44	600	UTe_2	U_7Te_{12}	2.1–2.2 ^c	65–70 ^c	^c Aggregated crystals

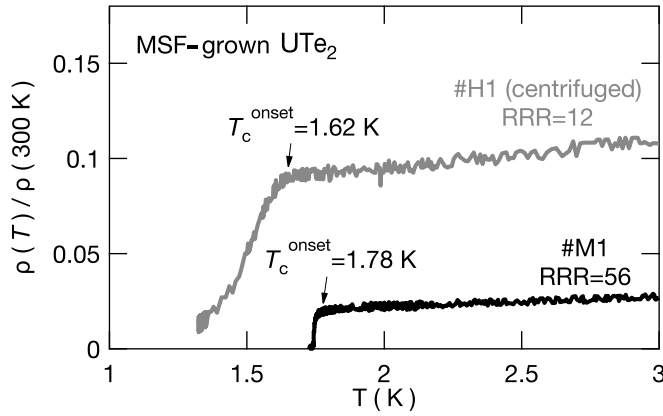


FIG. 2. Temperature dependence of normalized resistivity by $\rho(300\text{ K})$ along the a axis for the crystals picked from M1 and H1 in Table II.

Let us see the stoichiometric $\text{Te}/\text{U} = 2.0$ batches of M1 and H1 in Table II. As shown in Fig. 2, a crystal of UTe_2 picked from M1 shows a sharp SC transition at 1.78 K, and the RRR value for the crystal was 56, which is a relatively high value as compared with the CVT-grown crystals of SC1 and SC2. To test a dry process of removing the salt, the salt mixture of H1 was centrifuged. For this procedure, the quartz ampule was, for a short time of about 30 min, reheated to 700 °C. Although the crystals of UTe_2 could be cleanly extracted, the RRR value became worse, the T_c decreased, and the SC transition became broad. Probably, the quality of crystals may be degraded because of redissolution by reheating and/or rapid cooling by centrifugation. After this, to extract the crystals from the MSF method, the salts were dissolved in water.

All the crystals obtained from M1, M2, M3, M4, and M5 were UTe_2 in the form of long flat plate with a length of up to ~ 20 mm, a width of ~ 2 mm, and a thickness of ~ 1 mm, but larger crystals often comprised several crystals aggregated together, which could be easily cleaved. For resistance measurements, single crystals of about 1 mm in length were selected from each batch. Figure 3 shows the temperature dependences of normalized resistivity $\rho(T)/\rho(300\text{ K})$ for the crystals from L1, L1, H2, M1, M2, M3, M4, and M5.

When T_f was set to 600 °C (or 700 °C) lower (or higher) than the melting point of the eutectic salt, the crystals of L1 and H2 tend to show a spatially inhomogeneous SC behavior (Fig. 3), i.e., the resistivity drops in several steps with different T_c . The lower RRR values for L1 and H2 than those for M1, M2, M3, M4, and M5 imply larger density of crystal defects or distribution of chemical composition. Therefore, to make crystals homogeneous, T_f was set to 650 °C, which is close to the melting point of the eutectic salt. As for the salt amount, there were no appreciable differences of RRR and T_c between M4 and M5, and the size of crystals was not varied. Therefore, the molar ratio of salt was roughly adjusted to 40–70 with regard to the amount of uranium in these experiments, except for the first batch of M6 (U_7Te_{12}).

Notably, the T_c values of 1.9–2.1 K for M2, M3, M4, and M5 are quantitatively higher than those for the MSF-grown M1, and the CVT-grown SC1 and SC2 samples. The RRR

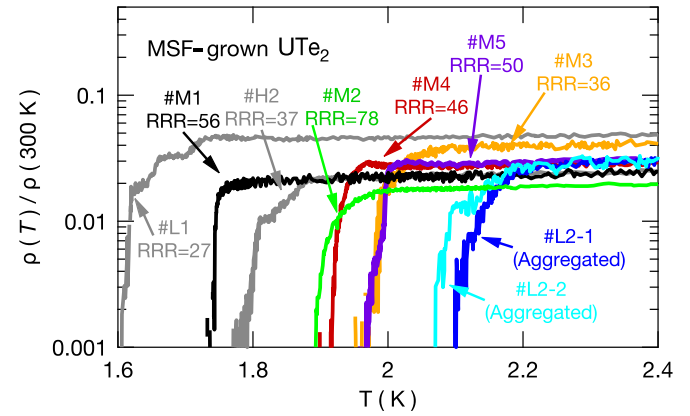
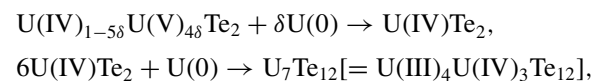


FIG. 3. Temperature dependence of normalized resistivity $\rho(T)/\rho(300\text{ K})$ for the crystals picked from L1, L2, H2, M1, . . . , M4, and M5 in Table II in the low temperature part. L2-1 and L2-2 indicate different aggregated crystals taken from L2.

values for the M2, M3, M4, and M5 batches are relatively high, although a small distribution of T_c might exist in some crystals. These results suggest that the crystals grown by the MSF method prepared from the U-rich ratio of $1.9 < \text{Te}/\text{U} < 2$ would be closer to the stoichiometry. Probably, such a fine-tuning to the stoichiometry would be realized from a surplus of uranium in the MSF, which acts as a reducing agent to avoid the generation of U^{5+} , and then assist to reduce the uranium deficiency in the crystals.

Concerning the L2 batch, although we could not find any large or clean crystals, we could pick some small, aggregated crystals of about 1 mm on each side. These crystals seemed to be aggregated in submillimeter scale and several texture patterns were visible on the facets. Perhaps, microscale phase separation did possibly occur during annealing at the lower $T_f = 600$ °C. In fact, the magnetization and specific heat measurements confirm a small amount of U_7Te_{12} by observation of the ferromagnetic transition at $T_{\text{Curie}} = 47\text{ K}$ in certain parts of these crystals. The resistivity $\rho(T)$ for L2-1 and L2-2 shows a small kink at T_{Curie} (not shown).

As shown in Fig. 3, the aggregated crystals exhibit the highest $T_c^{\text{onset}} = 2.1\text{--}2.2\text{ K}$, suggesting that the uranium deficiency δ in the percolated $\text{U}_{1-\delta}\text{Te}_2$ phase would be practically infinitesimal. These aggregated crystals also suggest that T_c may increase to 2.2 K, although such crystals have not yet been isolated. Thus, under extreme conditions that the adjacent U_7Te_{12} coexists, the stoichiometric UTe_2 would appear. This is probably because the following oxidation-reduction reactions in the MSF method are not sequential but occur almost simultaneously with an excess uranium:



where U(0) is uranium metal.

For this hypothesis, we again checked for the presence of UTe_2 crystals for the M6 batch. Then, an additional MSF run

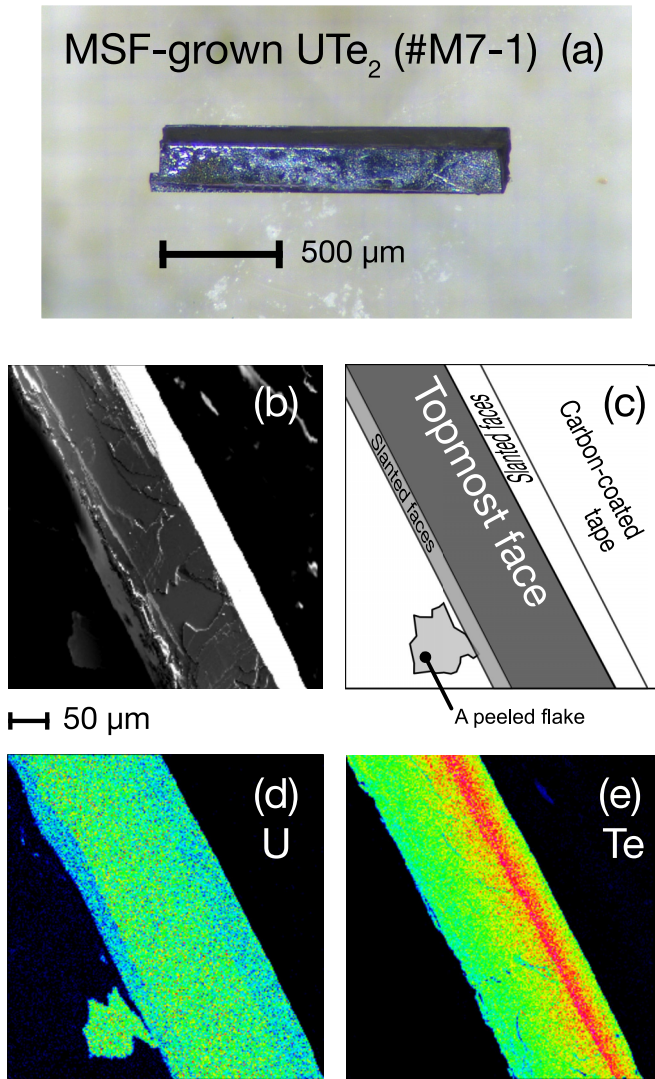


FIG. 4. (a) Photograph of a single crystal of UTe_2 picked from M7. The crystal is identical to the one of which electrical resistivity was measured (Fig. 5). (b) SEM image for the crystal and (c) the outline view of the micrograph, and EPMA-analyzed elemental mapping images for (d) uranium and (e) tellurium, respectively.

with an increased amount of salt was attempted as M6a in Table II. In this growth, as expected, several millimeter-sized UTe_2 crystals were found separately from the major U_7Te_{12} crystal product. Although they are small in size, the resistivity for an isolated crystal shows high $T_c = 2.1$ K and the high RRR value of 130, as shown later in Fig. 5(b). Therefore, as a working hypothesis, the stoichiometric UTe_2 can be obtained with an extremely reducing condition in a certain amount of MSF.

Even in the case of M7, while most of the crystals were U_7Te_{12} , several crystals of UTe_2 could be found, which were small in size, about 1 mm long and 0.2 mm in diameter, as shown in Fig. 4(a). The chemical composition is identified as UTe_2 with an accuracy of 1% using EPMA. The SEM image of the crystal is shown in Fig. 4(b), and its schematic outline is shown in Fig. 4(c). No compositional inhomogeneity was observed on the top surface of the

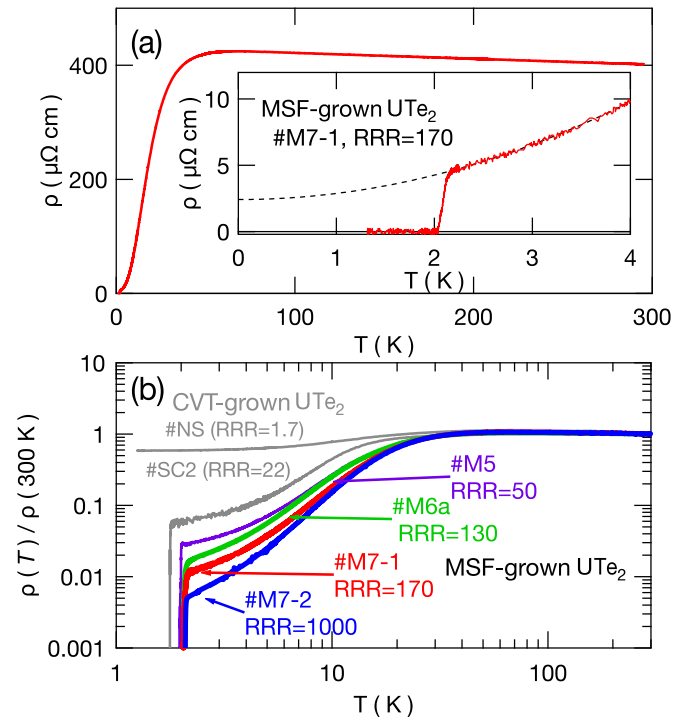


FIG. 5. (a) Temperature dependence of resistivity along the a axis for a crystal picked from M7 in Table II. The inset shows a magnified plot of the low temperature part. The RRR value at the room temperature is also indicated. The dotted curve represents the fitted curve of $\rho(T) = AT^2 + \rho(0)$ in the range of $T_c \leq T \leq 4$ K. (b) Temperature dependence of normalized resistivity $\rho(T)/\rho(300 \text{ K})$ for the crystals picked from M6a and M7. M7-2 indicate another crystal taken from M7. For comparison, the data for the crystals of the CVT-grown NS and SC2 in Table I and the MSF-grown M5 in Table II are also shown.

crystals in the EPMA-analyzed elemental mapping images for uranium and tellurium, as shown in Figs. 4(d) and 4(e), respectively. Stripelike brightness in Figs. 4(d) and 4(e) is not an intrinsic issue and is attributed to tilting angles between the detector and crystal facets. The visibility or invisibility of small, peeled flakes on the carbon-coated tape in Figs. 4(d) and 4(e) is only a matter of detection sensitivity and is not essential.

As shown in Fig. 5(a), the crystal (M7-1) exhibits a SC transition at $T_c^{\text{onset}} = 2.1$ K and RRR value of 170, which are categorized into the highest- T_c class. The $\rho(0)$ value for this crystal is $2.4 \mu\Omega \text{ cm}$, indicating the lower density of scattering centers for conduction electrons, that is, probably the considerably lower density of uranium vacancies than in the crystals grown by the CVT method. Notably, another crystal (M7-2) found in M7 shows the highest RRR value of about 1000, as shown in Fig. 5(b). Thus, at least, the RRR values for MSF-grown UTe_2 crystals are greatly improved compared with those for the CVT-grown crystals. Indeed, using these MSF-grown UTe_2 , de Haas-van Alphen oscillation has been observed for the first time [29] to demonstrate a long mean free path without impurity scatterings.

TABLE III. Typical values of the crystallographic parameters for UTe_2 crystals grown by the CVT method (NS and SC1/SC2) and MSF method (M7). Experimental uncertainty in parentheses includes deviations obtained for samples.

	NS	SC1/SC2	M7
Lattice parameters (\AA)			
a	4.1600(2)	4.1618(5)	4.1606(4)
b	6.1219(4)	6.1355(7)	6.1337(4)
c	13.9476(9)	13.9698(13)	13.9729(10)
Fractional coordinates			
U z	0.13545(5)	0.13520(4)	0.13515(3)
Te1 z	0.29755(5)	0.29780(10)	0.29794(5)
Te2 y	0.24895(5)	0.24910(3)	0.24907(11)
Site occupancy			
U	0.962(2)	0.993(5)	1.001(3)
B_{eq}^a			
U	0.614	0.513	0.500
Te1	0.661	0.576	0.561
Te2	0.712	0.529	0.534
Reliability factors ^b			
R_1	0.0192	0.0309	0.0178
wR_2	0.0367	0.0586	0.0419

^aEquivalent isotropic atomic displacement parameter is defined as $B_{\text{eq}} = 8\pi^2/3[U_{11}(aa^*)^2 + U_{22}(bb^*)^2 + U_{33}(cc^*)^2]$, where U_{ij} is experimentally obtained anisotropic atomic displacement tensor.

^b R_1 and wR_2 are unweighted and weighted agreement factors, respectively.

C. Crystallography

UTe_2 is orthorhombic and has a unique structure with space group of $Immm$ (71) [4,30,31]. In this crystal structure, U, Te(1), and Te(2) atoms occupy $4i$ ($mm2$), $4j$ ($mm2$), and $4h$ ($m2m$) sites, of which fractional coordinates are represented as $(0, 0, z)$, $(\frac{1}{2}, 0, z)$, and $(0, y, \frac{1}{2})$, respectively. Table III shows the crystallographic parameters for the NS, SC1/SC2, and M7-1 crystals determined by single-crystal XRD. The fractional coordinates and anisotropic atomic displacement parameters are determined, considering secondary extinction effect during the refinements. Moreover, considering the uranium deficient tendency in UTe_2 NS samples [20], the site occupancy of the uranium site for all the samples was fitted during the structural refinements.

As reported by Haga *et al.* [20], the lattice parameters of SC2 were slightly larger than those of NS shown in Table III, although the difference in lattice parameters between SC1 and SC2 samples was hardly discernible. Here, the values for NS and SC1/SC2 samples are obtained from the previously reported data [20], but revised by taking into account the site occupancy. Moreover, the difference in the lattice parameters between the SC2 and M7 crystals is barely discernible. There are also no specific changes in the bond lengths.

When the reliability factor R_1 was attempted to minimize through XRD profile fittings to vary the site occupancies [20], the amount of uranium site occupancy in the NS crystal can be estimated to be $\sim 4\%$, whereas the amount of uranium defects in the SC1/SC2 sample is 1% or less within the experimental uncertainty of 0.3 to 0.5%. Note that there was no such occupancy dependence of R_1 in both Te sites. From

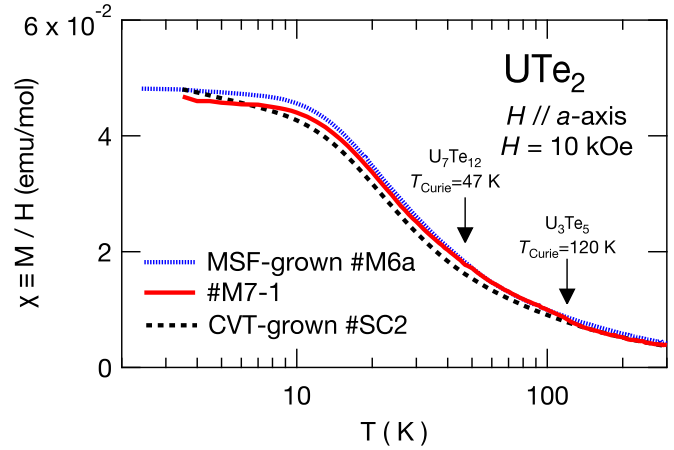


FIG. 6. Temperature dependence of magnetic susceptibility for the CVT-grown SC2, and the MSF-grown M6a and M7-1 crystals of UTe_2 with the application of an external field of 10 kOe along the a axis.

the same analysis, the occupancy of the uranium sites in the M7 crystal can be estimated to be as close as possible to 1 as listed in Table III. Although it is difficult to detect the occupancy difference among SC1, SC2, and M7 from the XRD experiments, the existence of an additional Curie-Weiss term of SC2 at low temperature, as shown in the next section, may be indicative of a small amount of uranium defect. Thus the U deficiency in the SC samples is estimated to be less than 1%, and it would be important to remove as much of this small amount of U vacancies as possible to increase T_c .

D. Magnetization and specific heat

Figure 6 shows the magnetic susceptibility $\chi \equiv M/H$ with the application of an external field of $H = 10$ kOe along the a axis, which is the magnetic easy axis. As for the M6a crystal shown in Fig. 6, there is a slight kink at 47 K, which corresponds to the ferromagnetic transition of U_7Te_{12} . The amount of U_7Te_{12} in the M6a crystal is estimated to be very small, considerably less than 0.01%.

As for M7-1, the magnetic susceptibility deviates upward just slightly from that for SC2, which is below ~ 120 K. This would correspond to a faint trace of ferromagnetic component with $T_{\text{Curie}} \sim 120$ K. The trace can be U_3Te_5 , although such a trace was not found by single-crystal XRD, EPMA, and resistivity measurements. U_3Te_5 is an orthorhombic semiconductor in the space group $Pnma$ and is reported to be a ferromagnet with an ordered moment of about $0.95\mu_B/U$ below $T_{\text{Curie}} \approx 120$ K [32]. Because of the high sensitivity of magnetometry, a small ferromagnetic inclusion could be detected, which was estimated as 0.2% of the molar amount, at most, for M7-1. The faint trace of U_3Te_5 suggests that the growth condition of M7 may be on the verge of further reduction of U_7Te_{12} , i.e., $5U(\text{III})_4U(\text{IV})_3Te_{12} + U(0) \rightarrow 12U(\text{III})_2U(\text{IV})Te_5$.

At low temperatures below ~ 10 K, the SC2 crystal shows a small Curie-Weiss-like increase in susceptibility. Such an additional increase of magnetic susceptibility along the a axis has been widely observed in CVT-grown UTe_2 crystals [1,15,33]. Assuming an anisotropic paramagnetism of

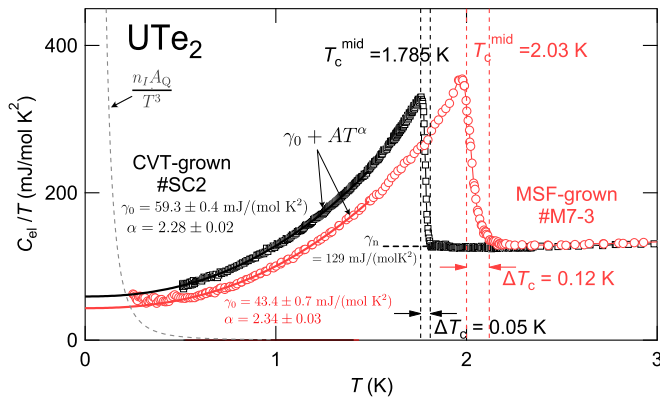


FIG. 7. Temperature dependence of electronic specific heat for the CVT-grown SC2 and MSF-grown M7-3 crystals of UTe_2 . The dashed curve is an estimate of nuclear Schottky contribution $n_l A_Q / T^3$ from ^{235}U nuclei (see text).

a free uranium ion, the low temperature Curie-Weiss term can be attributed to 1% of impurities [18]. Since such a behavior is suppressed in the M6a and M7-1 crystals, the Curie-Weiss-like behavior at low temperatures in the CVT-grown UTe_2 probably originates from local spins caused by uranium defects, i.e., $[\text{V}_\text{U}]_8\text{U}_{46}^{5+}$. The present observations suggest that the low-temperature Curie-Weiss term is sample dependent and absent in samples with low residual resistivity. In the absence of uranium defects, the magnetic susceptibility for UTe_2 will approach an enhanced value and become almost temperature independent as the temperature is lowered, as often observed in heavy fermion compounds. In addition, note that there is no apparent ferromagnetic fluctuation. Since the Curie-Weiss-like behavior driven by U vacancies at low temperatures is not caused by separated impurity phase, the additional slow spin dynamics because of such local spins could be microscopically observed by muon spin relaxation/rotation [34] and NMR [35] experiments.

As for the specific heat measurement, another crystal M7-3 of UTe_2 with $T_c^{\text{onset}} = 2.1$ K in resistivity was selected, of which the RRR value was ~ 260 . The electronic specific heat divided by temperature for the M7-3 crystal in the low temperature range is shown in Fig. 7. The phonon contribution is subtracted by Debye model with the Debye temperature of $T_D = 200$ K. For comparison, the data for the SC2 crystal grown by the CVT method is also plotted.

A large specific heat jump ΔC is seen at $T_c^{\text{mid}} = 2.03$ K, which proves the bulk superconductivity at higher T_c in the MSF-grown UTe_2 crystal of M7. Here, T_c^{mid} is defined as the midpoint between the onset and the peak temperatures of the specific heat jump. As often observed, the T_c^{mid} appears to be a bit smaller than the onset T_c in resistivity. Although the temperature width $\Delta T_c = 0.12$ K for the M7-3 crystal means a certain distribution of T_c , which is slightly larger than $\Delta T_c = 0.05$ K for the SC2 crystal, there was no multistep SC transition as seen in several literatures [16,36].

The specific heat jump at T_c for the MSF grown crystal of M7-3 can be estimated to be $\Delta C / (\gamma_n T_c) \simeq 1.75$, where $\gamma_n = 129$ mJ/(mol K^2) is the Sommerfeld coefficient in the

normal state. This $\Delta C / (\gamma_n T_c)$ value is larger than the weak coupling BCS limit of 1.43 and agrees with previous results reported on samples with T_c higher than 1.7 K [17]. Indeed, for the CVT-grown SC2 crystal with lower $T_c \simeq 1.8$ K, the specific heat jump $\Delta C / (\gamma_n T_c) \simeq 1.54$ was smaller than that for M7-3. Note that the γ_n values for both SC2 and M7-3 crystals are almost the same, regardless of the different T_c .

As seen in Fig. 7, the C_{el}/T for M7-3 approaches a constant below ~ 0.5 K, and it appears to slightly increase below ~ 0.3 K, which may be due to nuclear Schottky contribution by 0.72% ^{235}U nuclei (nuclear spin $I = \frac{7}{2}$ and the quadrupolar moment $Q = 4.1$ barns [37]) in the natural U sample. When the local symmetry of U site is lowered from cubic, the nuclear quadrupolar interactions cannot be ignored even for such a low abundance, as discussed by Cairns *et al.* [17]. The nuclear quadrupolar contribution can be expressed as $n_l A_Q / T^3$, where n_l is the isotopic density. Here, A_Q is given as follows [38–40]:

$$A_Q = \frac{1}{360} I(2I-1)(2I+2)(2I+3)(1+\eta^2/3)(\hbar v_Q)^2 / k_B,$$

where $v_Q = (e^2 q Q / h) \{3/[2I(2I-1)]\}$ is the nuclear quadrupolar frequency, where eq is the maximal component of electrical field gradient (EFG) tensor, and η is the asymmetric factor of EFG tensor. For example, $e^2 q Q / h \simeq 200$ MHz and $\eta = 0$ are experimentally obtained for the U sites in the antiferromagnetic state of cubic UO_2 [41]. In this UO_2 case, the cubic U symmetry becomes very slightly distorted due to a simultaneous $3k$ -type quadrupolar ordering with the antiferromagnetic ordering below $T_N = 30.8$ K. In the case of tetragonal USb_2 , $e^2 q Q / h \sim 2000$ MHz and $\eta = 0$ are roughly estimated for the local tetragonal U sites [42]. Although the actual EFG parameters are expected to be larger for the orthorhombic U site in UTe_2 , tentatively assuming the same values of $e^2 q Q / h$ and η as in USb_2 , a rough estimate of $n_l A_Q \sim 0.6$ mJ K/mol is obtained, of which contribution is drawn in Fig. 7. Thus the A_Q term in UTe_2 would be significant in the lowest T region.

The correct estimation of the electronic contribution in the low temperatures is important both for the identification of the possible residual density states and for the understanding of the SC mechanism of UTe_2 by probing the low-energy excitation. To estimate the residual electronic specific heat coefficient γ_0 ($T \rightarrow 0$) in the SC state, the C_{el}/T data were fitted to $\gamma_0 + AT^\alpha$ in the T range of 0.5–1.5 K, where the nuclear Schottky contribution would be suppressed. The obtained γ_0 values are 43.4 ± 0.7 and 59.3 ± 0.4 mJ/(mol K^2) for the M7-3 and SC2 crystals, which correspond to the γ_0/γ_n ratios of 33% and 46%, respectively. The temperature power α for both crystals seems to be slightly different from T^2 , which is expected in the point-node SC case. The γ_0/γ_n ratio for the M7-3 crystal is a relatively low value among the reported values [13,15,18]. Although the residual γ_{res} ratio is reported to be about 20% of the $\gamma_n = 121$ mJ/(mol K^2) for the best crystal with $T_c = 2$ K grown by the CVT method [15], these crystals were prepared from depleted U metal with the lower ^{235}U abundance of $< 0.3\%$. The estimates of residual

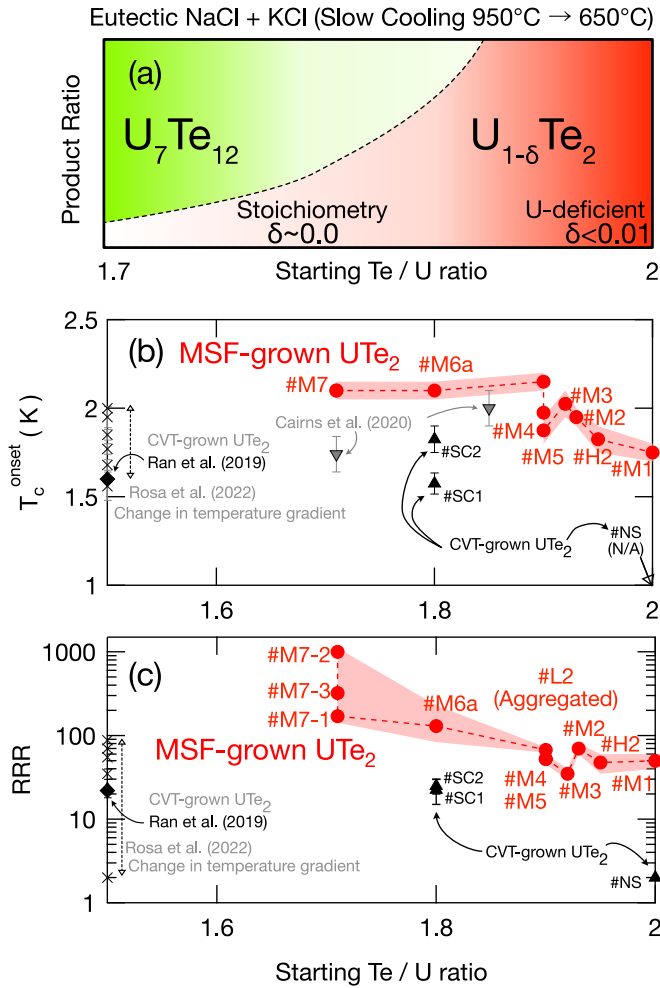


FIG. 8. (a) Schematic diagram of the crystals grown by the MSF method prepared from the various Te/U ratio. (b) T_c^{onset} and (c) RRR values versus the starting Te/U ratio plots for the obtained UTe_2 crystals. For comparison, the data for CVT grown crystals in this work and the literature [1,15,17] are also plotted.

γ_0 may be affected by the differences in the isotopic density of ^{235}U .

IV. SUMMARY

The schematic diagram of the crystals grown by the MSF method is illustrated in Fig. 8(a). The T_c and RRR values for various batches are plotted against the starting Te/U ratio. For comparison, the data for the CVT-grown crystals of NS, SC1, and SC2 and the data in the literature are plotted together in Figs. 8(b) and 8(c).

When the starting ratio is selected to be $1.9 < \text{Te}/U \leq 2$ with $T_f = 650$ °C, the crystals of $U_{1-\delta}Te_2$ can be mainly formed. Here, the U-deficiency δ appears to be as small as or smaller than that grown by the CVT method, which was estimated as $\delta \leq 0.01$ for the SC sample with $T_c = 1.9$ K [20]. Note that the CVT-grown sample NS from the nominal $\text{Te}/U = 2$ ratio was $\delta \simeq 0.04$ for the non-SC sample [20]. In the case of MSF, the higher T_c is observed for the crystal grown from the Te/U ratio deviating more from 2, as shown in Fig. 8(b). A similar trend may be seen even in the case of CVT,

but the data are highly distributed. In the CVT case, not only the Te/U ratio but also the temperature gradient seems to be important. Indeed, as Rosa *et al.* reported [15], optimization of the temperature gradient yields the high-quality crystal (RRR = 88) with $T_c = 2$ K.

In the case of MSF, such an excess of uranium would be effective in preventing $U_{1-\delta}Te_2$ from oxidizing and creating vacancies of the uranium sites. As the excess amount of uranium further increases, the hexagonal U_7Te_{12} phase partially appears. It seems that UTe_2 crystals without any defects can be obtained under such an extreme condition where $U_{1-\delta}Te_2$ ($\delta \ll 0.01$) and U_7Te_{12} coexist. The largest RRR value was recorded for the crystal picked from the M7 batch, as shown in Fig. 8(c). The magnetometry for the M7 crystal detected a small inclusion of a ferromagnetic component that seems to originate from U_3Te_5 , which is a further reduced product of U_7Te_{12} . According to our working hypothesis that the stoichiometric UTe_2 can be obtained under an extreme reducing condition, we are currently working on further optimizing the growth conditions.

Thus the MSF method is a promising technique for crystal growth of SC UTe_2 to control the T_c value and prevent any disorder caused by uranium vacancies. The MSF method would also be useful for various uranium chalcogenides, because it is applicable at relatively low temperatures to avoid volatilization of the constituent chalcogens.

ACKNOWLEDGMENTS

We would like to acknowledge D. Aoki and S. Ikeda for stimulating discussions and helpful comments. This work was partially supported by JSPS KAKENHI Grants No. JP16KK0106, No. JP19K03726, No. JP20H00130, No. JP20KK0061, and No. JP20K20905. This work was also financially supported by the JAEA Fund for Exploratory Researches (Houga fund).

APPENDIX: SINGLE CRYSTAL GROWTH BY CVT METHOD

The quartz tube was etched and smoothed on the inside with hydrofluoric acid. Approximately 20–50 mg of iodine (purity 99.999%, Furuuchi Chemical Co., Tokyo, Japan) was packed in a vacuum capillary in advance, which was broken open by shaking it in a vacuum-sealed quartz tube containing uranium and tellurium metals, that were weighed to a given ratio of Te/U. The quartz tube with an inner and outer diameter of 15 and 18 mm, respectively, was vacuum sealed in a length of about 200 mm. The quartz ampule was inserted into a two-zone horizontal electric tube-furnace (ARF2-370-50KC, Asahi-Rika Co., Ltd., Chiba, Japan). For prereaction to make the polycrystalline form, the temperature of the entire furnace was slowly increased to 950 °C over 24 h and kept at the temperature for another 24 h. As an inverse transport to clean the growth zone, the charge zone of the quartz tube was set at a lower temperature (T_L) and the growth zone at a higher temperature (T_H), leaving it for several days. Then, the temperatures were set to the growth condition (i.e., the opposite temperature gradient between T_L and T_H) and left for 10 days. After the above procedure,

both ends were set to T_L , and the temperatures were then lowered to room temperature. Single crystals of several millimeters in size were obtained from the middle to the T_L

end of the quartz tube. The crystals were rinsed with ethanol to remove trace iodine and immediately dried in a vacuum atmosphere.

- [1] S. Ran, C. Eckberg, Q.-P. Ding, Y. Furukawa, T. Metz, S. R. Saha, I.-L. Liu, M. Zic, H. Kim, J. Paglione, and N. P. Butch, Nearly ferromagnetic spin-triplet superconductivity, *Science* **365**, 684 (2019).
- [2] G. Knebel, W. Knafo, A. Pourret, Q. Niu, M. Vališka, D. Braithwaite, G. Lapertot, M. Nardone, A. Zitouni, S. Mishra, I. Sheikin, G. Seyfarth, J.-P. Brison, D. Aoki, and J. Flouquet, Field-reentrant superconductivity close to a metamagnetic transition in the heavy-fermion superconductor UTe_2 , *J. Phys. Soc. Jpn.* **88**, 063707 (2019).
- [3] S. Ran, I.-L. Liu, Y. S. Eo, D. J. Campbell, P. M. Neves, W. T. Fuhrman, S. R. Saha, C. Eckberg, H. Kim, D. Graf, F. Balakirev, J. Singleton, J. Paglione, and N. P. Butch, Extreme magnetic field-boosted superconductivity, *Nat. Phys.* **15**, 1250 (2019).
- [4] S. Ikeda, H. Sakai, D. Aoki, Y. Homma, E. Yamamoto, A. Nakamura, Y. Shiokawa, Y. Haga, and Y. Ōnuki, Single crystal growth and magnetic properties of UTe_2 , *J. Phys. Soc. Jpn.* **75**, 116 (2006).
- [5] D. Braithwaite, M. Vališka, G. Knebel, G. Lapertot, J. P. Brison, A. Pourret, M. E. Zhitomirsky, J. Flouquet, F. Honda, and D. Aoki, Multiple superconducting phases in a nearly ferromagnetic system, *Commun. Phys.* **2**, 147 (2019).
- [6] D. Aoki, F. Honda, G. Knebel, D. Braithwaite, A. Nakamura, D. Li, Y. Homma, Y. Shimizu, Y. J. Sato, J.-P. Brison, and J. Flouquet, Multiple superconducting phases and unusual enhancement of the upper critical field in UTe_2 , *J. Phys. Soc. Jpn.* **89**, 053705 (2020).
- [7] S. Ran, H. Kim, I.-L. Liu, S. R. Saha, I. Hayes, T. Metz, Y. S. Eo, J. Paglione, and N. P. Butch, Enhancement and reentrance of spin triplet superconductivity in UTe_2 under pressure, *Phys. Rev. B* **101**, 140503(R) (2020).
- [8] W.-C. Lin, D. J. Campbell, S. Ran, I.-L. Liu, H. Kim, A. H. Nevidomskyy, D. Graf, N. P. Butch, and J. Paglione, Tuning magnetic confinement of spin-triplet superconductivity, *npj Quantum Mater.* **5**, 68 (2020).
- [9] G. Nakamine, S. Kitagawa, K. Ishida, Y. Tokunaga, H. Sakai, S. Kambe, A. Nakamura, Y. Shimizu, Y. Homma, D. Li, F. Honda, and D. Aoki, Superconducting properties of heavy fermion UTe_2 revealed by ^{125}Te -nuclear magnetic resonance, *J. Phys. Soc. Jpn.* **88**, 113703 (2019).
- [10] G. Nakamine, K. Kinjo, S. Kitagawa, K. Ishida, Y. Tokunaga, H. Sakai, S. Kambe, A. Nakamura, Y. Shimizu, Y. Homma, D. Li, F. Honda, and D. Aoki, Anisotropic response of spin susceptibility in the superconducting state of UTe_2 probed with ^{125}Te -NMR measurement, *Phys. Rev. B* **103**, L100503 (2021).
- [11] H. Fujibayashi, G. Nakamine, K. Kinjo, S. Kitagawa, K. Ishida, Y. Tokunaga, H. Sakai, S. Kambe, A. Nakamura, Y. Shimizu, Y. Homma, D. Li, F. Honda, and D. Aoki, Superconducting order parameter in UTe_2 determined by knight shift measurement, *J. Phys. Soc. Jpn.* **91**, 043705 (2022).
- [12] D. Aoki, A. Nakamura, F. Honda, D. Li, Y. Homma, Y. Shimizu, Y. J. Sato, G. Knebel, J.-P. Brison, A. Pourret, D. Braithwaite, G. Lapertot, Q. Niu, M. Vališka, H. Harima, and J. Flouquet, Unconventional superconductivity in heavy fermion UTe_2 , *J. Phys. Soc. Jpn.* **88**, 043702 (2019).
- [13] D. Aoki, A. Nakamura, F. Honda, D. Li, Y. Homma, Y. Shimizu, Y. J. Sato, G. Knebel, J.-P. Brison, A. Pourret, D. Braithwaite, G. Lapertot, Q. Niu, M. Vališka, H. Harima, and J. Flouquet, Spin-triplet superconductivity in UTe_2 and ferromagnetic superconductors, Proceedings of the International Conference on Strongly Correlated Electron Systems, *JPS Conf. Proc.* **30**, 011065 (2020).
- [14] S. Ran, I.-L. Liu, S. R. Saha, P. Saraf, J. Paglione, and N. P. Butch, Comparison of two different synthesis methods of single crystals of superconducting uranium ditelluride, *J. Vis. Exp.* **173**, e62563 (2021).
- [15] P. F. S. Rosa, A. Weiland, S. S. Fender, B. L. Scott, F. Ronning, J. D. Thompson, E. D. Bauer, and S. M. Thomas, Single thermodynamic transition at 2 K in superconducting UTe_2 single crystals, *Commun. Mater.* **3**, 33 (2022).
- [16] S. M. Thomas, C. Stevens, F. B. Santos, S. S. Fender, E. D. Bauer, F. Ronning, J. D. Thompson, A. Huxley, and P. F. S. Rosa, Spatially inhomogeneous superconductivity in UTe_2 , *Phys. Rev. B* **104**, 224501 (2021).
- [17] L. P. Cairns, C. R. Stevens, C. D. O'Neill, and A. Huxley, Composition dependence of the superconducting properties of UTe_2 , *J. Phys.: Condens. Matter* **32**, 415602 (2020).
- [18] D. Aoki, J.-P. Brison, J. Flouquet, K. Ishida, G. Knebel, Y. Tokunaga, and Y. Yanase, Unconventional superconductivity in UTe_2 , *J. Phys.: Condens. Matter* **34**, 243002 (2022).
- [19] V. P. Mineev, Low temperature specific heat and thermal conductivity in superconducting UTe_2 , *J. Phys. Soc. Jpn.* **91**, 074601 (2022).
- [20] Y. Haga, P. Opletal, Y. Tokiwa, E. Yamamoto, Y. Tokunaga, S. Kambe, and H. Sakai, Effect of uranium deficiency on normal and superconducting properties in unconventional superconductor UTe_2 , *J. Phys.: Condens. Matter* **34**, 175601 (2022).
- [21] D. Coleman and P. Lacy, The phase equilibrium diagram for the KCl-NaCl system, *Mater. Res. Bull.* **2**, 935 (1967).
- [22] H. Hashitani, A. Hoshino, and T. Adachi, High-Purity Uranium Metal Standard Sample (JAERI-U4) for Determination of Uranium, JAERI-M Reports (in Japanese) No. 5343, Japan Atomic Energy Research Institute, Tokai, Naka, Ibaraki, Japan, 1973.
- [23] G. M. Sheldrick, Crystal structure refinement with *SHELXL*, *Acta Crystallogr. C* **71**, 3 (2015).
- [24] D. R. Boehme, M. C. Nichols, R. L. Snyder, and D. P. Matheis, An investigation of the tellurium-rich uranium tellurides using x-ray powder diffraction, *J. Alloys Compd.* **179**, 37 (1992).
- [25] K. Serrano and P. Taxil, Electrochemical reduction of trivalent uranium ions in molten chlorides, *J. Appl. Electrochem.* **29**, 497 (1999).
- [26] K. Serrano and P. Taxil, Electrochemical nucleation of uranium in molten chlorides, *J. Appl. Electrochem.* **29**, 505 (1999).

- [27] K. Serrano, P. Taxil, O. Dugne, S. Bouvet, and E. Puech, Preparation of uranium by electrolysis in chloride melt, *J. Nucl. Mater.* **282**, 137 (2000).
- [28] O. Tougait, M. Potel, and H. Noël, Characterization of the binary uranium and thorium tellurides U_7Te_{12} and Th_7Te_{12} , *Inorg. Chem.* **37**, 5088 (1998).
- [29] D. Aoki, H. Sakai, P. Opletal, Y. Tokiwa, J. Ishizuka, Y. Yanase, H. Harima, A. Nakamura, D. Li, Y. Homma, Y. Shimizu, G. Knebel, J. Flouquet, and Y. Haga, First observation of de Haas–van Alphen effect and Fermi surfaces in unconventional superconductor UTe_2 , *J. Phys. Soc. Jpn.* **91**, 083704 (2022).
- [30] A. Haneveld and F. Jellinek, The crystal structure of stoichiometric uranium ditelluride, *J. Less-Common Met.* **21**, 45 (1970).
- [31] K. Stöwe, Contributions to the crystal chemistry of uranium tellurides: III. Temperature-dependent structural investigations on uranium ditelluride, *J. Solid State Chem.* **127**, 202 (1996).
- [32] O. Tougait, M. Potel, and H. Noël, Crystal structure and magnetic properties of the binary triuranium pentatelluride U_3Te_5 , *J. Solid State Chem.* **139**, 356 (1998).
- [33] W. Knafo, M. Nardone, M. Vališka, A. Zitouni, G. Lapertot, D. Aoki, G. Knebel, and D. Braithwaite, Comparison of two superconducting phases induced by a magnetic field in UTe_2 , *Commun. Phys.* **4**, 40 (2021).
- [34] S. Sundar, S. Gheidi, K. Akintola, A. M. Côté, S. R. Dunsiger, S. Ran, N. P. Butch, S. R. Saha, J. Paglione, and J. E. Sonier, Coexistence of ferromagnetic fluctuations and superconductivity in the actinide superconductor UTe_2 , *Phys. Rev. B* **100**, 140502(R) (2019).
- [35] Y. Tokunaga, H. Sakai, S. Kambe, Y. Haga, Y. Tokiwa, P. Opletal, H. Fujibayashi, K. Kinjo, S. Kitagawa, K. Ishida, A. Nakamura, Y. Shimizu, Y. Homma, D. Li, F. Honda, and D. Aoki, Slow electronic dynamics in the paramagnetic state of UTe_2 , *J. Phys. Soc. Jpn.* **91**, 023707 (2022).
- [36] I. M. Hayes, D. S. Wei, T. Metz, J. Zhang, Y. S. Eo, S. Ran, S. R. Saha, J. Collini, N. P. Butch, D. F. Agterberg, A. Kapitulnik, and J. Paglione, Multicomponent superconducting order parameter in UTe_2 , *Science* **373**, 797 (2021).
- [37] P. B. Dorain, C. A. Hutchison, and E. Wong, Paramagnetic resonance absorption in uranium (III) chloride and the nuclear spin, magnetic dipole moment, and electric quadrupole moment of uranium-233, *Phys. Rev.* **105**, 1307 (1957).
- [38] B. Bleaney, Nuclear specific heats in paramagnetic salts, *Phys. Rev.* **78**, 214 (1950).
- [39] N. E. Phillips, Nuclear quadrupole and electronic heat capacities of bismuth, *Phys. Rev.* **118**, 644 (1960).
- [40] M. Krusius and G. Pickett, Calorimetric determination of the nuclear quadrupole interaction in arsenic, *Solid State Commun.* **9**, 1917 (1971).
- [41] K. Ikushima, S. Tsutsui, Y. Haga, H. Yasuoka, R. E. Walstedt, N. M. Masaki, A. Nakamura, S. Nasu, and Y. Ōnuki, First-order phase transition in UO_2 : ^{235}U and ^{17}O NMR study, *Phys. Rev. B* **63**, 104404 (2001).
- [42] H. Kato, H. Sakai, K. Ikushima, S. Kambe, Y. Tokunaga, D. Aoki, Y. Haga, Y. Ōnuki, H. Yasuoka, and R. E. Walstedt, Direct observation of ^{235}U NMR in an itinerant 5f electron system, USb_2 , *J. Phys. Soc. Jpn.* **73**, 2085 (2004).